

Numerical Simulation of a Laboratory-Scale Turbulent V-flame

J. B. Bell, M. S. Day, I. G. Shepherd, M. Johnson, R. K. Cheng,
V. E. Beckner, M. J. Lijewski, J. F. Grear

Lawrence Berkeley National Laboratory
Berkeley, California, 94720 USA

corresponding author: Marcus S. Day
address: Lawrence Berkeley National Laboratory
Mail Stop 50A-1148
One Cyclotron Road
Berkeley, CA 94720-8142 USA
fax: (510) 486-6900
email: MSDay@lbl.gov

colloquium: 13. Miscellaneous (in lieu of Turbulent Flames,
because an author is co-chairing that colloquium)

running title: Laboratory-Scale Turbulent V-flame

text word count: 6050 words, determined by counting words

abstract:	170	(not included in total)
main text:	3450	
references:	330	
figure 1 and caption:	190	
figure 2 and caption:	180	
figure 3 and caption:	310	
figure 4 and caption:	190	
figure 5 and caption:	190	
figure 6 and caption:	170	
figure 7 and caption:	360	
figure 8 and caption:	360	
figure 9 and caption:	160	
figure 10 and caption:	160	

Abstract

We present three-dimensional, time-dependent simulations of the flowfield ($12 \times 12 \times 12$ cm) in a laboratory-scale rod-stabilized premixed turbulent V-flame. The simulations are performed using an adaptive time-dependent low Mach number combustion algorithm based on a second-order projection formulation that conserves both species mass and total enthalpy. The methodology incorporates detailed chemical kinetics and a mixture model for differential species diffusion. Methane chemistry and transport are modeled using the DRM-19 (20-species, 84-reaction) mechanism derived from the GRI-Mech 1.2 mechanism along with its associated thermodynamics and transport databases. The adaptive mesh refinement dynamically resolves the flame and turbulent structures. A separate nonreacting computation is performed to characterize the inflow turbulence. The numerical procedures for the simulations of the reacting flow and the inlet turbulence are described. Detailed comparisons with experimental measurements show that the computational results provide a good prediction of the mean flame angle, flame spread and turbulence flowfield. It is expected that a higher level of mesh refinement will improve the fidelity of the computation to resolve the internal structures of the flamelets.

Keywords

premixed turbulent combustion, numerical simulation, V-flames

1 Introduction

Premixed turbulent flames are of increasing practical importance and remain a significant research challenge in the combustion community. A variety of flame configurations have been studied experimentally and they can be categorized by the flame stabilization mechanism. For example, the previous Combustion Symposium includes studies by Sattler et al. [1] of a turbulent V-flame, Shepherd et al. [2] of a swirl-stabilized flame, Most et al. [3] of a bluff-body stabilized flame, and Chen et al. [4] of Bunsen and stagnation flames. Modern experimental diagnostics as well as theory (see, for example, Peters [5]) have made substantial progress in understanding basic flame physics and developing models that can be used for engineering design. However, the inability of theory to deal with the complexity of realistic chemical kinetics in a turbulent flow field, and the present limitations in experimental diagnostics to resolve 3D flame properties, represent major obstacles to continued progress.

Numerical simulation offers the potential to augment theory and experiment and so overcome the limitations of standard approaches in analyzing laboratory-scale flames. However, for premixed turbulent combustion, the excessive computation costs of incorporating detailed transport and chemical kinetics have necessitated compromises in the fidelity or scope of simulations. Simulation of laboratory-scale systems typically involves models for subgrid-scale turbulent fluctuations and for turbulence-flame interactions. Approaches based on large eddy simulation (LES) fall into this class, and show improved potential for predictive capabilities compared to traditional tools based on the Reynolds-averaged Navier-Stokes equations; however, LES approaches still require a model for the speed of flame propagation in a turbulent field, in addition to the LES treatment of the fluid turbulence itself. See, for example, Pitsch and Duchamp de Lageneste [6] who develop an LES algorithm combined with a flamelet model based on a filtered G-equation.

There have been a number of computational studies that attempt to resolve detailed chemical kinetics and transport instead of incorporating an explicit flame speed model. However, these types of studies have been severely restricted in spatial extent and dimensionality. Baum et al. [7] studied 2D turbulent flame interactions for detailed hydrogen chemistry, and Haworth et al. [8] have examined the effect of inhomogeneous reactants for 2D propane-air flames using detailed propane chemistry. More recently Tanahashi et al. [9, 10] performed direct numerical simulations

of turbulent, premixed hydrogen flames in three dimensions with detailed hydrogen chemistry. Bell et al. [11] performed a similar study for a turbulent methane flame. However, both these 3D simulation studies were restricted to very small ($\mathcal{O}(1)$ cm) idealized configurations. Significantly, the computed flame configurations were unstable because spatial excursions of the flame from turbulent acceleration toward the inflow boundary would invalidate the inflow idealization when the boundary is eventually reached. As a result, the computed flames could not evolve long enough to establish a stable configuration comparable to an experimentally observable turbulent flame.

In this paper, we study a turbulent rod-stabilized premixed methane V-flame in a statistically stationary, physically stable configuration. For the calculations, we employ an adaptive low Mach number model that includes detailed transport and chemical kinetics. No explicit models for turbulence or turbulence-chemistry interactions are employed in the simulations, and the quasi-steady flames that result are compared with a similar laboratory V-flame experiment. This work represents both an extension of the results presented in [11] to a physically realizable configuration ($\mathcal{O}(10)$ cm), and a first step toward simulating a laboratory-scale turbulent premixed flame with enough fidelity to allow detailed understanding of combustion chemistry and pollutant formation. We summarize our approach to the simulation, and present a validation of the approach with experimental data, by comparing mean and fluctuating velocity and scalar fields, and estimates of the flame surface density. We discuss plans for follow-on research in terms of detailed chemical and flowfield analysis useful for enhancing the understanding of the combustion and pollutant chemistry in the experimental flame.

2 Experimental Configuration and Diagnostics

A time-averaged photograph of the laboratory V-flame experiment appears as an inset in Figure 1. A methane/air mixture at equivalence ratio $\phi = 0.7$ exits a 5 cm diameter circular nozzle with a nearly top hat velocity profile with a mean axial velocity of 3 m/s. Turbulence is introduced by a perforated plate mounted 9 cm upstream of the nozzle exit. The integral length scale of the turbulence measured by PIV (Particle Imaging Velocimetry) at the nozzle exit is $\ell_t \sim 3.5$ mm. The fluctuation intensity is slightly anisotropic at 7.0% and 5.5% in the axial and radial directions respectively, relative to the mean axial velocity. The flame is stabilized by a 2 mm diameter rod

spanning the nozzle width at its exit. The visible flame extends 20 cm or more downstream from the rod.

The PIV system consists of a double-pulse New Wave Solo PIV laser (120 mJ) at 532 nm and a Kodak/Red Lake ES 4.0 digital camera with 2048 by 2048 pixel resolution. The field of view was approximately 12 cm by 12 cm and the pixel resolution was 0.065 mm/pixel. A cyclone type particle seeder was used to seed the main air flow with 0.4–0.6 μm (Sumitomo AKP-15) Al_2O_3 particles. Data acquisition and analysis were performed on 448 image pairs using software developed by Wernet [12]. The two-pass, adaptive cross-correlation interrogation regions of 32×32 pixels with final 50% overlapping gave a velocity field spatial resolution of approximately 1 mm. The data sets comprise the reacting flow (in a plane normal to the rod at the center) and non-reacting flow without the rod to characterize turbulence produced by the turbulence generator.

3 Computational Model

A schematic of the computational domain is shown in Figure 1. Our strategy is to characterize independently the turbulence generation in the nozzle using nonreacting simulations to provide a boundary condition for the reacting flow simulation. This simulation is based on a low Mach number formulation of the reacting flow equations. The methodology treats the fluid as a mixture of perfect gases, and uses a mixture-averaged model for differential species diffusion, ignoring Soret and Dufour effects¹. The chemical kinetics are modeled using the DRM-19 methane mechanism with 20 species and 84 fundamental reactions. Our basic discretization algorithm combines a symmetric operator-split coupling of chemistry and diffusion processes with a density-weighted approximate projection method for incorporating the velocity divergence constraint arising from the low Mach number formulation. This basic integration scheme is embedded in a parallel adaptive mesh refinement (AMR) algorithm. Our approach to adaptive refinement is based on a block-structured hierarchical grid system composed of nested rectangular grid patches. The adaptive algorithm is second-order accurate in space and time, and discretely conserves species mass and enthalpy. The reader is referred to [13] for details of the low Mach number model and its numerical implementation and to

¹Note to reviewer: The references describing this method and its applications are available at: http://seesar.lbl.gov/CCSE/Publications/pub_date.html

[11] for previous applications of this methodology to the simulation of premixed turbulent flames.

3.1 Nozzle Characterization

As a turbulence model is not used in these simulations the characterization of the turbulence inlet conditions is a critical aspect of these simulations. We assume that the fluid in the nozzle is an isothermal, incompressible, homogeneous gas. From the experimental data, we know that the exit flow essentially has a top hat profile with very thin viscous boundary layers at the interior pipe wall. From this observation, we make the simplifying assumption that the turbulence generation in the central region of the nozzle is not strongly influenced by the side walls of the nozzle. By a Taylor hypothesis argument, we obtain an initial characterization of the turbulence in the nozzle from the temporal evolution of an array of perturbed jets whose diameter and spacing are obtained from turbulence generation plate used in the experiment. Specifically, we simulate a triply-periodic cube, 5 cm on a side initialized with a hexagonal array of 3.2 mm jets spaced 4.8 mm apart with a velocity chosen so that the average velocity in the domain is the mean nozzle exit flow velocity. The simulation is performed on a 256^3 grid using a dynamic viscosity of $1.6 \cdot 10^{-5}$ m²/s, corresponding to a methane-air mixture at 300 K. The flow is evolved for 0.03 seconds (i.e., the residence time of the nozzle flow). At $t = 0.03$ s, the integral length scale and turbulence intensity of the resulting simulated flow agrees with the measured quantities reported above, including the observed anisotropy.

As a further check on the assumption made in characterizing the turbulence generated in the nozzle and the role of the nozzle walls on the turbulent generation process, we performed an additional simulation of the nozzle flow using a 3D time-dependent compressible gas dynamics code. This method, which uses an embedded-boundary representation of the domain geometry [14], was used to simulate the flow in the nozzle and includes a representation of the turbulence generation plate. We accumulated turbulent statistics from this simulation and compared them to the periodic incompressible flow simulation described earlier. Away from the nozzle walls, the turbulent intensities matched very well. Near the walls the rms fluctuation level in the axial velocity increases to 100% over its mean value in a region approximately 1.25 mm from the nozzle wall. The rms fluctuations in the radial velocity show a corresponding 80% decrease. These two observations are consistent with the solid wall boundary conditions, and conservation of momentum.

We computed fits to the variation in turbulent intensities near the walls and used them to shape the turbulence computed from the incompressible simulation described above.

3.2 Reacting Flow Simulation Setup

The computational domain for the reacting flow simulation is a cube, 12 cm on a side, with the nozzle exit centered on the lower face. The sides of this domain are approximated as slip walls and the top is a constant pressure outflow boundary. The reactant stream inflow profile is formed by superimposing a mean flow at 3 m/s on the turbulent fluctuations from the incompressible computation. The flame stabilization rod is modeled as a 3 mm wide no-flow strip at the nozzle exit. We specify an air coflow of 1.5 m/s into the bottom of the domain outside the nozzle to control the shear layers that form between the ambient gas and the outer layer of the reactant flow downstream of the inflow. The solution in the reacting flow region is initialized with room-temperature stagnant air throughout the domain, and a small hot region just above the rod. As the flow evolves, the heated air ignites a flame near the inlet, and the flame surface trails downstream within the flow of the turbulent reactant. The resulting flame is evolved until it reaches statistical equilibrium.

For a premixed methane flame at a fuel equivalence ratio of $\phi = 0.7$, the thermal thickness is approximately 600 μm . The Kolmogorov scale of the inflowing turbulent reactants is approximately 220 μm . Even with our adaptive low Mach number simulation capability, it was not possible with the available computing resources to evolve the reacting flow field at the refinement level necessary to resolve all the reaction and viscous length scales in the problem. Our approach is to determine empirically the grid resolution necessary to obtain converged flame and velocity field statistics that allow direct comparisons with experimental values. The initial computed evolution is carried out with a 2-level adaptive grid hierarchy, where a factor of two refinement from the base grid of 96^3 dynamically tracks regions of high vorticity and chemical activity (the flame front). After a quasi-steady flame is achieved, an additional factor of two refinement was placed at the flame surface and high vorticity regions. The solution was evolved approximately 21 ms further in time with this fine-grid resolution of $\Delta x = 312.5 \mu\text{m}$ collecting the flame surface and velocity statistics presented in the next section. The strategy resulted in approximately 12% of the 12^3 cm^3 domain being refined to the highest level. This is consistent with the physics of premixed turbulence flame where the

flame brush occupies a small volume. Convergence in the derived statistics was verified by analyzing similar data from the 2-level solution at $650\ \mu\text{m}$, and from a limited evolution at an additional factor-of-two refinement ($156.25\ \mu\text{m}$). The flame and velocity statistics presented in the following section were largely insensitive to refinement below $\Delta x_{\text{eff}} = 312.5\ \mu\text{m}$. The flame was evolved for a total of 132 ms, and the analysis was based on simulation data at 0.5 ms intervals. CPU requirements depended on the refinement strategy, but the computation progressed approximately $200\ \mu\text{s}$ per hour on 128 processors of a parallel computer (IBM SP RS/6000 with 375 MHz processors). The total run, including the refinement study, generated approximately 6 TB of data for analysis. An image of the instantaneous flame surface at the $312.5\ \mu\text{m}$ resolution appears in Figure 2².

4 Experimental Comparisons

We focus our comparison on the overall flame brush properties and the mean and rms velocities obtained from PIV. Although the smallest grid of $312.5\ \mu\text{m}$ is only approximately half the thermal thickness of the wrinkled flame fronts, the comparison shows that the resolution is adequate for predicting the salient features this V-flame.

4.1 Scalar Flame Structure

Due to the large difference in Mie scattering intensities from the reactants and products, the instantaneous wrinkled flame front is clearly outlined on the PIV image (Figure 3b). Compared to a centerline slice of the methane concentration obtained from the simulation (Figure 3a) the wrinkling of the flame in the experiment and the computation show similar size and structure. To characterize the flame brush, the position of the flame fronts were obtained from 100 PIV images (e.g. Figure 3b) by an edge finding algorithm for rendering binarized images. Their average produces a map of the mean reaction progress, \bar{c} , where $\bar{c} = 0$ in reactants, and $\bar{c} = 1$ in the products. For the simulation data, we define an instantaneous progress variable $c = (\rho_u - \rho)/(\rho_u - \rho_b)$ where $\rho_{u,b}$ are the densities of the unburned and burned gas, respectively. Averaging c over a sample of slices through the computed flame defines an analogous \bar{c} for the computation.

The spreading rates of \bar{c} contours in Figure 4 indicate the growth of the experimental and the

²An animation of the computed flame surface is available at: <http://seesar.lbl.gov/CCSE/index.html>

computed flame brushes. The simulation shows good agreement up to approximately $z < 10$ cm at which point the computational results begin to exhibit the effect of the outflow imposed at $z = 12$ cm. The simulation and the experimental results have slightly different included angles. In the experiment, the $\bar{c} = 0.5$ contour forms an angle of approximately 11 deg with the vertical compared to 13 deg for the computation. (See below for further discussion of this issue.)

To provide a more detailed comparison of the flame brush growth, in Figure 5 we plot \bar{c} versus radial distance, x , at various downstream locations. These figures are corrected by shifting the computational profiles so that the $\bar{c} = 0.5$ points coincide. From the plot, we see that the computation can match the growth of the experimental flame brush thickness although the computational results predict a slightly wider flame brush than the experimental data indicates. This discrepancy may be attributable to differences in the spectral content of inflow turbulence.

The flame surface density, Σ , is often used to quantify the combustion intensity in low Mach number premixed flames. It increases as a result of flame front wrinkling by the turbulence and is therefore directly related to the burning rate of the turbulent flame. The analogue of this parameter in 2D slices, the flame front length to flame zone area ratio, Σ_{2D} , can be evaluated and compared for both the experimental and simulation data. The method given in [15] was used to obtain Σ_{2D} from the flame edges (described above) and from the corresponding 2D slices of the simulation data. In Figure 6, the flame surface density averaged over the entire experimental and simulated flame brushes are plotted as functions of the mean progress variable \bar{c} . The distributions are similar and well described by the relationship $\Sigma_{2D} = k\bar{c}(1 - \bar{c})$ which has been observed in many premixed flame configurations.

4.2 Velocity Comparisons

Figures 7 and 8 show, respectively, the mean radial ($\langle U \rangle$) and axial ($\langle W \rangle$) velocity components for the simulation and the experiment. Data from the simulation was averaged over approximately 21 ms, a time comparable to the reactant residence time, and to the large eddy turnover time at the nozzle. The $\bar{c} = 0.1$ and $\bar{c} = 0.9$ contours (dashed lines) are superimposed to indicate the flame zone locations. The computed and experimental velocity data shows good qualitative agreement. The simulation captures with remarkable fidelity the major features of the experimental data, i.e. flame generated outward deflection in the unburned gases, inward flow convergence and a centerline flow

acceleration in the burned gases.

The mean radial velocity, $\langle U \rangle$, is slightly larger in the burned region for the simulation than for the measured data, and weaker in the unburned region. The simulation also shows a slightly larger increase in the axial velocity, $\langle W \rangle$, in the burned gases. These small differences can be traced to difference in the inflow boundary conditions: the flow rate measured at the center of the nozzle is higher and has a thicker boundary layer than that of the simulation. It is probable that the higher velocity in the center of the nozzle is also responsible for the slightly narrower included V angle mentioned earlier. In auxiliary 2D simulations, the included angle in comparable V-flames was found to be sensitive to the coflow velocity and domain size. We are currently assessing the extent to which this sensitivity occurs, in three dimensions, and how it is affected by the presence of significant turbulence in the fuel stream.

Another difference observable in Figure 8 is the experimental centerline velocity deficit that is not shown by the simulation. This deficit is caused by the stabilizer wake; the simulations did not attempt a physically realistic representation of the rod. It will be noted, however, that the flame is entirely outside the wake and that its dynamics are therefore determined predominantly by its interaction with the reactant flow turbulence.

Figures 9 and 10 show computed and experimental fluctuations for the radial (U') and axial (W') velocities, again with \bar{c} contours superimposed to locate the flame. The agreement between the simulation and the experiment is, once again, very encouraging; the principal features of the fluctuations agree remarkably well. The velocities reported here are not conditioned by reference to the state of the scalar field. The largest fluctuations, therefore, occur within the flame zone due to the motion of the flame front such that burned and unburned gases are sampled at the same physical location. The major difference between the simulation and experiment is the increased intensity of the radial fluctuations in the simulation's flame.

5 Concluding Remarks

In this paper, we have presented a comparison between a three-dimensional, time-dependent simulation of a turbulent laboratory scale V-flame and data from a corresponding experiment. The simulations are performed using a low Mach number adaptive algorithm that incorporates detailed

chemistry and a mixture model for differential diffusion. A primary objective of this study was to determine, by direct comparison with experimental data, the refinement levels necessary to predict the overall scalar (flame brush) and turbulence (mean and rms) fields. The simulation was carried out in two parts. Inflow conditions were generated in a separate nonreacting simulation of the upstream turbulent flow produced by a perforated plate in a circular nozzle. For the reacting flow region, a $(12\text{ cm})^3$ domain was used. It was found that, with our low Mach number implementation, a 3-level adaptive grid hierarchy, with a finest-level grid spacing, $\Delta x = 312.5\ \mu\text{m}$, was capable of predicting with remarkable fidelity the major features of the experimental results. The mean flame angle was obtained within 2 degrees, and most of the key flow features (i.e., flame generated deflection of the unburned gases, inward convergence and axial acceleration of burned gases) were well-predicted by the simulation. This study confirms that our AMR low Mach number implementation is well-suited for simulating these types of laboratory flames.

We plan to augment this work to directly complement experiments in the study of premixed turbulent combustion. For example, we can validate the experimental approaches to approximating three-dimensional flame surface area from 2D PIV snapshots of the flame surface. With additional grid refinement localized to regions of the flame surface, we can more carefully quantify the instantaneous accelerations across the flame and assess the local burning velocities. We also plan to investigate the effects of flame stretch and curvature on these quantities as well as to generalize the types of diagnostics discussed in our earlier studies of premixed flames (cf. [16]). Finally, with additional chemical fidelity and the analysis tools developed in [17], we can interrogate the turbulence effects on fundamental combustion processes, and determine the production and transport characteristics of emissions.

References

- [1] Sattler, S. S., Knaus, D. A., and Gouldin, F. C., *Proc. Combust. Inst.*, 29:1785–1795 (2002).
- [2] Shepherd, I. G., Cheng, R. K., Plessing, T., Kortschik, C., and Peters, N., *Proc. Combust. Inst.*, 29:1833–1840 (2002).
- [3] Most, D., Dinkelacker, F., and Leipertz, A., *Proc. Combust. Inst.*, 29:1801–1806 (2002).
- [4] Chen, Y.-C., Kalt, P. A. M., Bilger, R. W., and Swaminathan, N., *Proc. Combust. Inst.*, pp. 1863–1871 (2002).
- [5] Peters, N., *Turbulent Combustion*, Cambridge University Press, Cambridge, UK, 2000.
- [6] Pitsch, H. and Duchamp De Lageneste, L., *Proc. Combust. Inst.*, pp. 2001–2008 (2002).
- [7] Baum, M., Poinso, T. J., Haworth, D. C., and Darabiha, N., *J. Fluid Mech.*, 281:1–32 (1994).
- [8] Haworth, D. C., Blint, R. J., Cuenot, B., and Poinso, T. J., *Combust. Flame*, 121:395–417 (2000).
- [9] Tanahashi, M., Fujimura, M., and Miyauchi, T., *Proc. Combust. Inst.*, 28:529–535 (2000).
- [10] Tanahashi, M., Nada, Y., Ito, Y., and Miyauchi, T., *Proc. Combust. Inst.*, 29:2041–2049 (2002).
- [11] Bell, J. B., Day, M. S., and Grcar, J. F., *Proc. Combust. Inst.*, 29:1987–1993 (2002).
- [12] Wernet, M. P., *Proceedings of the 18th International Congress on Instrumentation for Aerospace Simulation Facilities*, (1999), Toulouse, France.
- [13] Day, M. S. and Bell, J. B., *Combust. Theory Modelling*, 4:535–556 (2000).
- [14] Pember, R. B., Bell, J. B., Colella, P., Crutchfield, W. Y., and Welcome, M. W., *Proceedings of the Eleventh AIAA Computational Fluid Dynamics Conference*, pp. 948–958, June (1993).
- [15] Shepherd, I. G., *Proc. Combust. Inst.*, 22:373–379 (1996).

- [16] Bell, J. B., Brown, N. J., Day, M. S., Frenklach, M., Grcar, J. F., and Tonse, S. R., *Proc. Combust. Inst.*, 28:1933–1939 (2000).
- [17] Bell, J. B., Day, M. S., Grcar, J. F., Bessler, W. G., Schultz, C., Glarborg, P., and Jensen, A. D., *Proc. Combust. Inst.*, 29:2195–2202 (2002).

List of Figures

1	Schematic of the computation domain showing the division into the turbulence generation and reacting flow regions. A photograph of the laboratory experiment appears as an inset.	15
2	Simulated instantaneous flame surface	15
3	(a) Computed CH ₄ mole fraction, (b) Typical PIV image.	16
4	Comparison of \bar{c} contours. Left (red) is experiment; right (blue) is simulation	16
5	Experimental (line) and simulated (symbol) \bar{c} at four elevations: $z = 1, 3, 5, 7$ cm. Note the simulated results are shifted to compensate for differences in simulated and experimental V-angles	17
6	Experimental and simulated flame surface density	17
7	Mean transverse velocity (a) computed and (b) experimental.	18
8	Mean axial velocity (a) computed and (b) experimental.	18
9	Rms transverse velocity (a) computed and (b) experimental.	19
10	Rms axial velocity (a) computed and (b) experimental.	19

Figures

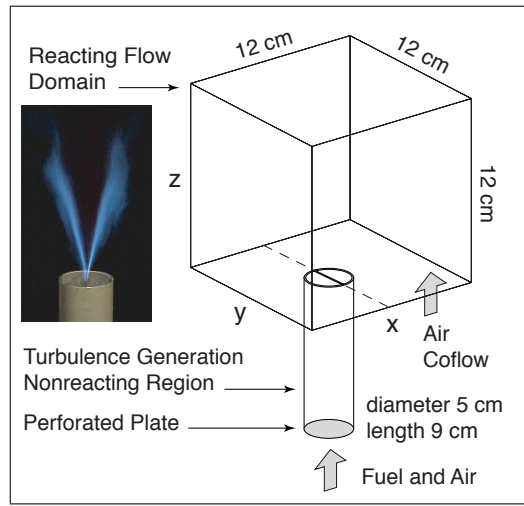


Figure 1: *Schematic of the computation domain showing the division into the turbulence generation and reacting flow regions. A photograph of the laboratory experiment appears as an inset.*

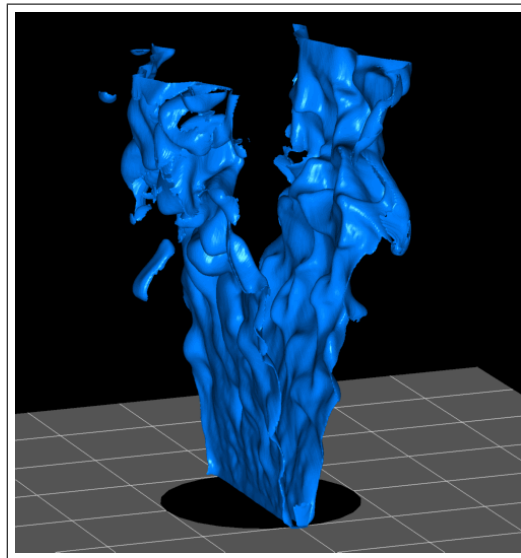


Figure 2: *Simulated instantaneous flame surface*

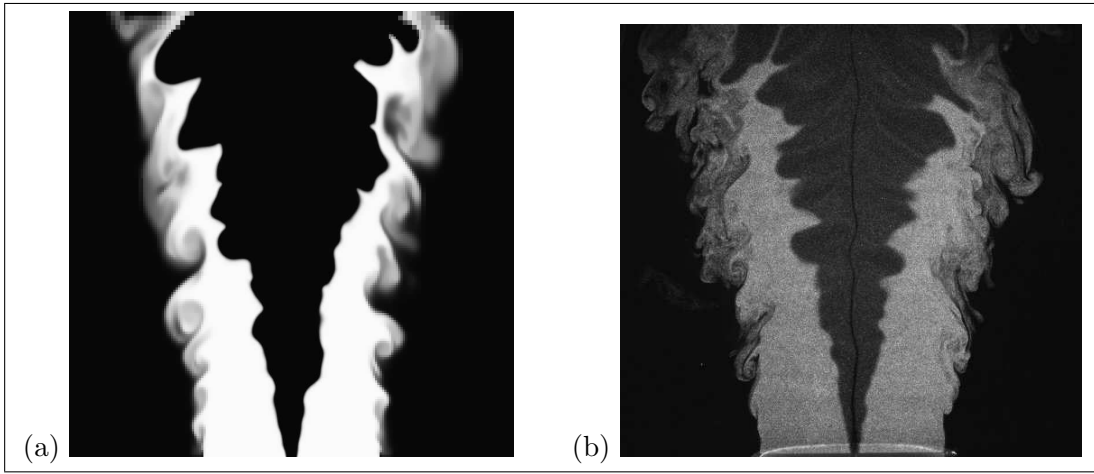


Figure 3: (a) Computed CH_4 mole fraction, (b) Typical PIV image.

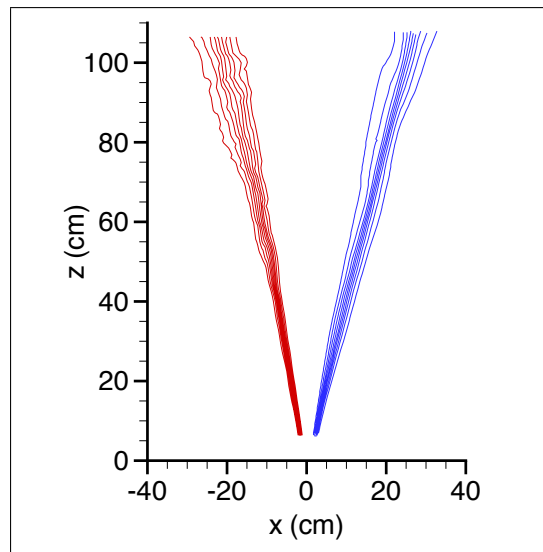


Figure 4: Comparison of \bar{c} contours. Left (red) is experiment; right (blue) is simulation

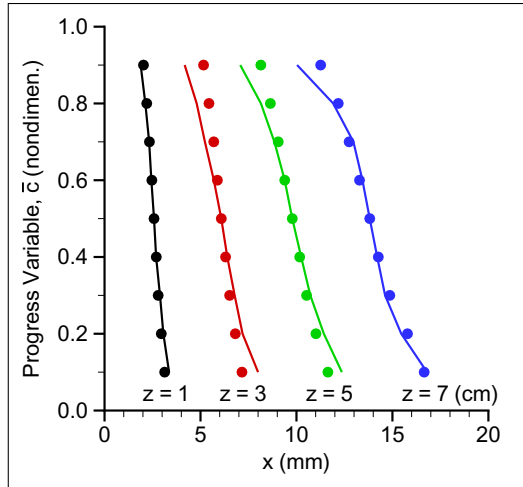


Figure 5: *Experimental (line) and simulated (symbol) \bar{c} at four elevations: $z = 1, 3, 5, 7$ cm. Note the simulated results are shifted to compensate for differences in simulated and experimental V -angles*

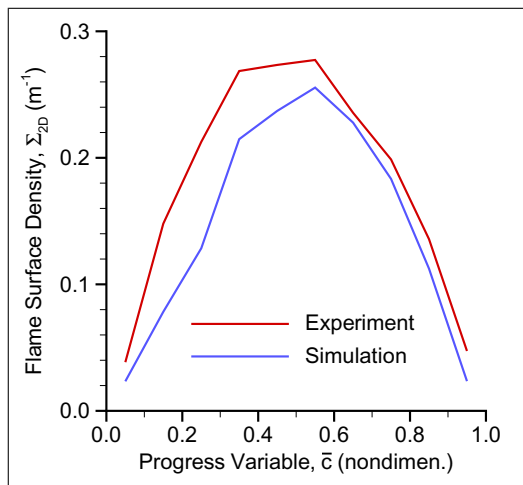


Figure 6: *Experimental and simulated flame surface density*

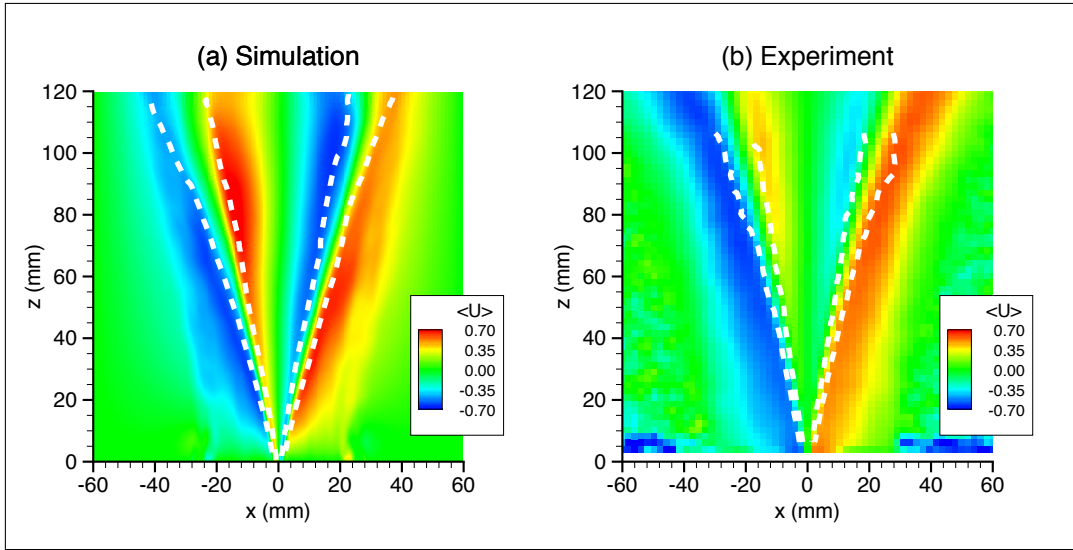


Figure 7: Mean transverse velocity (a) computed and (b) experimental.

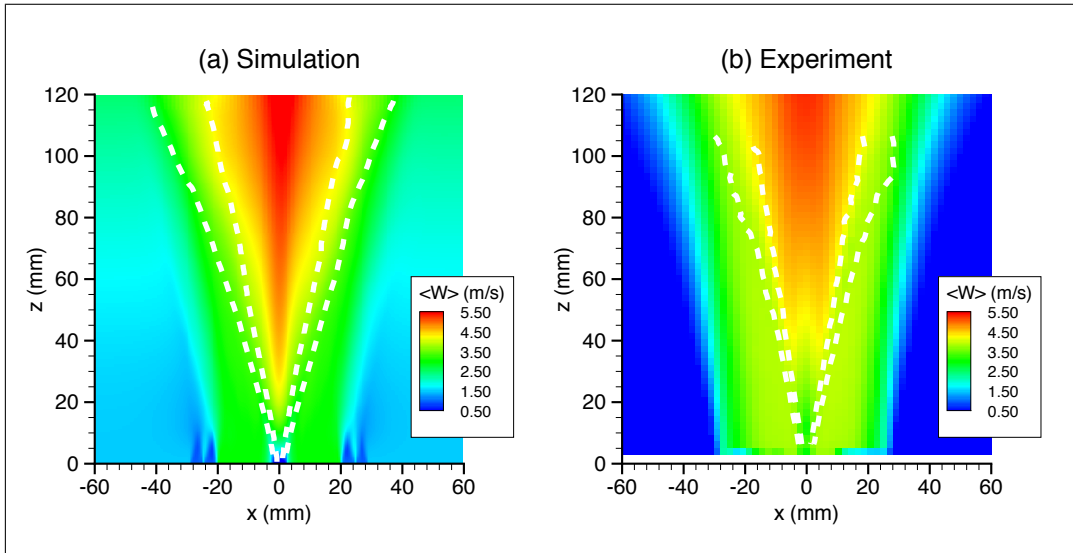


Figure 8: Mean axial velocity (a) computed and (b) experimental.

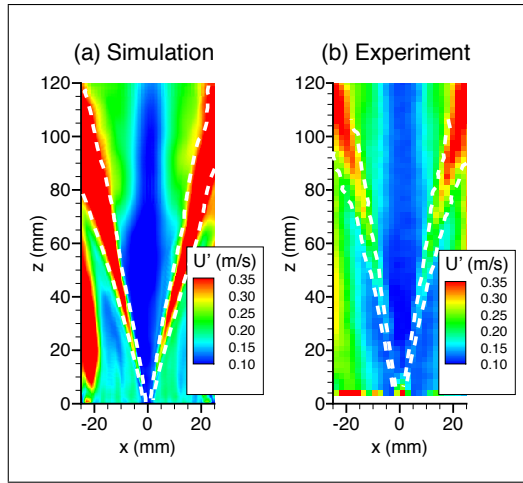


Figure 9: *Rms transverse velocity (a) computed and (b) experimental.*

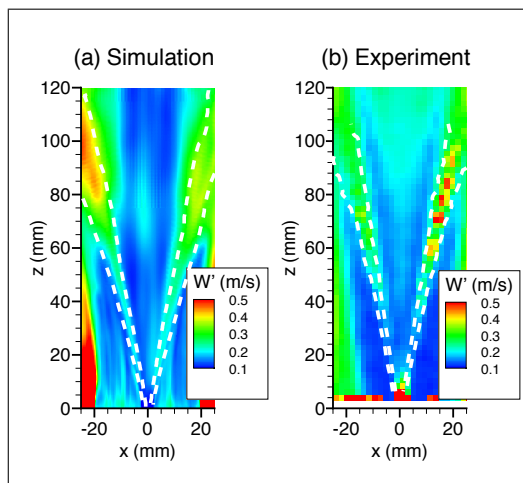


Figure 10: *Rms axial velocity (a) computed and (b) experimental.*